

Highlights

Feasibility of meteor surveying from a Venus orbiter

Apostolos A. Christou, Maria Gritsevich

- We use physics-based modelling to understand the properties of meteors in the upper atmosphere of Venus and to compare meteor survey efficiency from Earth orbit and from Venus orbit
- Venus meteors would be brighter and shorter-lived than Earth meteors, due to different atmospheric density scale heights
- Assuming similar meteoroid populations at the two planets, orbital meteor surveys would detect $1.5\times$ – $2.5\times$ more meteors per hour at Venus than at Earth

Feasibility of meteor surveying from a Venus orbiter

Apostolos A. Christou^{a,*}, Maria Gritsevich^{b,c}

^aArmagh Observatory and Planetarium, College Hill, Armagh BT61 9DG, Northern Ireland, United Kingdom

^bFaculty of Science, Gustav Hällströmin katu 2, FI-00014 University of Helsinki, Finland

^cInstitute of Physics and Technology, Ural Federal University, Mira str. 19, 620002 Ekaterinburg, Russia

ARTICLE INFO

Keywords:

Meteoroids

Meteors

Venus, atmosphere

Space vehicle instruments

ABSTRACT

Meteor and bolide phenomena caused by the atmospheric ablation of incoming meteoroids are predicted to occur at the planet Venus. Their systematic observation would allow to measure and compare the sub-mm to m meteoroid flux at different locations in the solar system. Using a physical model of atmospheric ablation, we demonstrate that Venus meteors would be brighter, shorter-lived, and appear higher in the atmosphere than Earth meteors.

To investigate the feasibility of meteor detection at Venus from an orbiter, we apply the SWARMS survey simulator tool to sets of plausible meteoroid population parameters, atmospheric models and instrument designs suited to the task, such as the Mini-EUSO camera operational on the ISS since 2019.


We find that such instrumentation would detect meteors at Venus with a 1.5× to 2.5× higher rate than at Earth. The estimated Venus-Earth detection ratio remains insensitive to variations in the chosen observation orbit and detector characteristics, implying that a meteor survey from Venus orbit is feasible, though contingent on the availability of suitable algorithms and methods for efficient on-board processing and downlinking of the meteor data to Earth.

We further show that a hypothetical camera onboard the upcoming *EnVision* mission to Venus similar to the ISS instrument should detect many times more meteors than needed for an initial characterisation of the large meteoroid population at 0.7 au from the Sun.

1. Introduction

Meteoroids that efficiently ablate in the Earth's atmosphere are broadly grouped into *streams* and *sporadics* (Campbell-Brown, 2007). Stream meteoroids were ejected from a parent comet or asteroid relatively recently - typically in the last 10^2 – 10^4 yr - and retain a dynamical memory of their birth so that they can be readily associated with a specific parent body (Valsecchi et al., 1999; Gritsevich et al., 2022). As these stream meteoroids approach Earth, they follow nearly parallel paths and manifest in the atmosphere as meteor showers, with the most intense ones dominating the flux of visible meteors for periods of a few days. Sporadic meteoroids, on the other hand, arrive at the Earth throughout the year from different directions and dominate the annually-averaged mass influx to our planet (Brown et al., 2008). Streams and sporadics are genetically related, as sporadics represent former stream meteoroids that have evolved to their current orbits through planetary gravitational scattering, solar-thermal radiation forces, and inter-particle collisions (Grün et al., 1985; Wiegert et al., 2009).

*Corresponding author

 Apostolos.Christou@armagh.ac.uk (A. A. Christou)

ORCID(s):

Observations of meteors hold the potential to characterise the flux of meteor-producing meteoroids - typically 0.1-1000 mm in size - across a range of heliocentric distances by systematically monitoring planetary atmospheres from orbit (Jenniskens, 2006; Christou et al., 2007, 2019). Being the planet with the nearest orbit to the Earth's, Venus naturally lends itself to this task. Theoretical and laboratory studies (McAuliffe, 2006; McAuliffe and Christou, 2006; Blaske et al., 2023) suggest that visible meteors readily occur at Venus, the brightest of which may even be detectable from Earth (Beech and Brown, 1995). While meteors are typically recorded using ground-based, upward-looking optical cameras, such an approach is impractical at Venus due to its thick, opaque atmosphere and harsh surface conditions. Conversely, the concept of a camera looking down on the planet from orbit is well-suited to meet this challenge.

Recent models of the terrestrial sporadic flux are calibrated against a diversity of datasets obtained at Earth: meteor counts obtained by radar, observations of zodiacal dust emission, meteoric metal abundances in the upper atmosphere or samples of unmelted micrometeorites (Wiegert et al., 2009; Nesvorný et al., 2010, 2011; Carrillo-Sánchez et al., 2016). Extrapolated to Venus, these models predict a similar overall mass influx to the terrestrial case ($\sim 30 \text{ t d}^{-1}$) (Frankland et al., 2017; Carrillo-Sánchez et al., 2020) as might perhaps be expected from consideration of the planetary sizes and the proximity of the orbits. The models also predict significant differences in the spatial and temporal distribution of the flux during the planetary year, owing to the different orbit shapes and orientations, rotation rates and obliquities of the rotation axis (Janches et al., 2020).

Obtaining meteor data at Venus will therefore allow to test models of the meteoroid influx in the inner solar system which are currently heavily-anchored to Earth observations. The same observations will also lead to the discovery of new meteoroid streams and the study by proxy of their cometary parent bodies, will test our understanding of ablation physics under non-terrestrial conditions and also help mitigate the risk of impact-induced damage to spacecraft (Christou and Vaubaillon, 2010; Schimmerohn et al., 2018; Krüger et al., 2021). The existence of Venusian meteors is also relevant to the interpretation of short-lived optical transients ("flashes") observed recently by the Japanese Exploration Agency's *Akatsuki* spacecraft (Lorenz et al., 2022; Blaske et al., 2023). Similar transients have been reported during an earlier ground-based search for lightning flashes (Hansell et al., 1995) while a feature recorded by the Pioneer Venus Orbiter Ultraviolet Spectrometer instrument in 1979 was interpreted as the ~ 900 -km long trail of a grazing meteor (Huestis and Slanger, 1993).

As *Akatsuki* continues its atmospheric monitoring mission, Venus features in the deep space exploration plans of India, the European Space Agency, the United States, China (Widemann et al., 2023) as well as private sector initiatives (Seager et al., 2022) presenting potential opportunities for conducting meteor surveys at Venus. Despite holding clear advantages over ground-based surveys (Bouquet et al., 2014), the record of spaceborne meteor detection has until now been the result of serendipity, a case in point being the set of 29 Leonids recorded by the US Ballistic

Missile Defense Organization Midcourse Space eXperiment (MSX) satellite in 1997 (Jenniskens et al., 2000) when the estimated Zenithal Hourly Rate of that shower (ZHR; the theoretical number of shower meteors seen by an observer under ideal conditions, see e.g. Beech, 2006) was ~ 100 , 1–2 orders of magnitude less than that of the 1999–2002 Leonid storms (with ZHR in the 1000s; e.g. Soja et al., 2015) and more typical of annually-recurring showers such as the August Perseids or December Geminids (Jenniskens, 1994; Jenniskens et al., 2016).

This paper takes a quantitative look at the feasibility of observing meteors in the atmosphere of the planet Venus from an orbiter spacecraft. Given the present level of maturity in the field, it is appropriate to produce quantitative predictions to support future instrument development and to optimize the design of orbital meteor surveys. We focus mainly on the sporadic component of the meteoroid flux which is better constrained from the Earth observations and available models. While Venus-crossing meteoroid streams should exist in abundance at Venus (Beech, 1998; Christou, 2004a,b, 2010), the characteristics of the meteor showers they produce will generally differ from one stream to the other. We note that successful forecasting of year-on-year variations of shower activity at Earth often relies on the availability of prior observations of the same shower (Asher et al., 1999; McNaught and Asher, 1999; Vaubaillon et al., 2005a,b, 2023) which are not available for Venus. Meteor rate predictions for the unobserved Venus showers will therefore require a case-by-case treatment, taking into account the specific properties of the parent body, the meteoroid production function and the orbital history of the stream. In the last Section of this paper, the contribution of shower meteors to the overall number of detections expected from an orbital platform at Venus is extrapolated from the observational record of terrestrial activity in order to estimate the overall detection rate of a hypothetical camera on-board the future ESA *EnVision* orbiter.

In the following Section, we introduce a theoretical framework to understand the principal differences between terrestrial and Venusian meteors, enhancing previous findings obtained by numerically solving the ablation equations. Our analytical treatment of atmospheric ablation relies on specific approximations in the regime where meteoroid ablation has begun before significant deceleration sets in. This limits the size of a meteoroid treatable by our model, the limit in terms of meteor brightness being roughly equivalent to the faintest fireballs (i.e. approximately -4 absolute magnitude). While the general theory remains valid for larger meteoroid sizes, our survey simulations primarily focus on fainter meteors treatable by the approximate theory. This is because detection statistics are dominated by these fainter meteors, where the relevant mathematical expressions are much simpler than the corresponding exact forms. In Sections 3 & 4, we complement the analytical results with simulations of meteor surveying by suitable instrument models at Earth and Venus orbit using the sophisticated SWARMS code. Section 5 details the further application of SWARMS to understand how our earlier conclusions depend on instrument characteristics and meteoroid environment parameters. Finally, in Section 6 we summarize our main findings and outline potential avenues for follow-on studies.

Table 1
Notation used for the principal quantities in this paper.

Symbol	Units	Description
ρ_m, h, V, M, S	kg m ⁻³ , km, km s ⁻¹ , g, m ²	Meteoroid bulk density, height, speed, mass and cross-sectional area during atmospheric entry
ρ_0, M_0, V_0	kg m ⁻³ , g, km s ⁻¹	Meteoroid pre-atmospheric density, mass and speed
γ	degrees	Angle of meteoroid flight path to horizon
ρ_a, h_0	kg m ⁻³ , km	Atmospheric density and scale height
ρ_0	kg m ⁻³	Atmospheric density at $h=0$
$\bar{\rho}=\rho_a\rho_0^{-1}$	–	Normalised atmospheric den- sity
μ	–	Meteoroid shape coefficient
H^*	J kg ⁻¹	Effective enthalpy of destruc- tion
c_d	–	Atmospheric drag coefficient
c_h	–	Heat transfer coefficient
$\sigma=c_h(c_d H^*)^{-1}$	s ² m ⁻²	Meteoroid ablation coefficient
$A_0=S_0\rho_m^{2/3}M_0^{-2/3}$	–	Meteoroid shape factor
E_{kin}	J	Meteoroid kinetic energy
I, m	W	Meteor luminous intensity and stellar magnitude
h_{max}, I_{max}	km, W	Meteor height and luminous intensity at maximum bright- ness
h_{end}	km	Meteor end height
τ, τ_G	–	Instantaneous and global lu- minous efficiency factors

2. Model of the ablation of small meteoroids

Meteors emit light via collisional excitation of line emission as the ablated meteoric vapour interacts with atmospheric species (Bronshten, 1983; Ceplecha et al., 1998). In the 200–700 nm spectral region, the strongest spectral lines correspond to meteoric species such as Mg, Fe and Na rather than atmospheric species such as O or N (Millman, 1963; Bronshten, 1983; Ceplecha et al., 1998; Carbary et al., 2003). We therefore expect the meteor integral radiation at these wavelengths to be only weakly dependent on atmospheric composition. Strong near-infrared atmospheric lines such as OI at 777 nm are sometimes found in spectra of fast meteors (so-called “type Y” spectra; Ceplecha et al., 1998) however such meteors are rare in the observational record. Therefore, in this paper we assume that meteor light intensity is proportional to the rate of ablative mass loss from the meteoroid and that empirically-derived scalings used to obtain one from the other are atmosphere-independent. The contribution of atmospheric emissions to meteor light and its variation with atmospheric composition is an interesting open question beyond the scope of the present study.

During atmospheric entry, a meteoroid with mass M and speed V generates a meteor of luminous intensity I given by:

$$I = -\tau \frac{dE_{\text{kin}}}{dt} \quad (1)$$

where the luminous efficiency τ is the fraction in the instantaneous meteoroid loss rate of kinetic energy $E_{\text{kin}}=0.5MV^2$ converted into light. The rate of energy dissipation is evaluated by simultaneously solving for ablative mass loss and deceleration (e.g. Bronshten, 1983)

$$M \frac{dV}{dt} = -\frac{1}{2}c_d\rho_a V^2 S \quad (2)$$

$$H^* \frac{dM}{dt} = -\frac{1}{2}c_h\rho_a V^3 S \quad (3)$$

where H^* is the effective enthalpy of destruction, c_d and c_h are respectively drag and heat transfer coefficients, ρ_a is the atmospheric density at the corresponding height, and S is the meteoroid cross section presented to the airflow.

For meteoroids small enough to ablate completely before noticeable deceleration sets in, meteor intensity can be determined from mass loss alone (Eq. 3) and τ can be replaced by the so-called global luminous efficiency τ_G , the fraction of the initial kinetic energy converted to luminous energy. In the special case of an exponential atmosphere with density scale height h_0 , energy dissipation in Eq. 1 can be expressed analytically, using the height equation $dh/dt = -V \sin \gamma$ and the successive transformations $t \rightarrow h \rightarrow \bar{\rho}=\exp(-h/h_0)$ to re-write Eq. 3 as

$$\frac{dM}{dh} = \frac{M_0 K}{h_0(1-\mu)} \bar{\rho}(1-K\bar{\rho})^{\mu/(1-\mu)} \quad (4)$$

where

$$K = \frac{(1-\mu)c_h\rho_0 S_0 h_0 V_0^2}{2H^* \sin \gamma M_0} \quad (5)$$

and M_0 , S_0 & V_0 are the meteoroid's pre-atmospheric mass, cross-section and speed respectively, ρ_0 is defined through the relationship $\rho_a=\rho_0\bar{\rho}$ and γ is the flight path angle relative to the horizon. Our analytical treatment is derived from that used previously (Gritsevich, 2009, 2010; Gritsevich and Koschny, 2011; Gritsevich et al., 2012; Bouquet et al., 2014) as the basis for a least-square-minimisation process to retrieve the meteoroid atmospheric deceleration, mass loss and luminosity history from observations of the meteor flight and determine its outcome. Although we do not consider non-exponential atmospheric profiles in this study, the procedure can also incorporate an arbitrary atmospheric model using the recently introduced atmospheric height correction method (Lyytinen and Gritsevich, 2016).

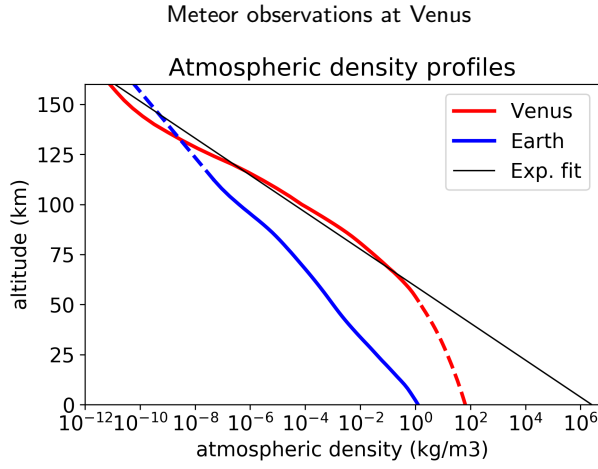


Figure 1: Atmospheric density profiles for Earth (Minzner, 1976) and for Venus (Seiff, 1983). The dashed part of the Earth profile represents an extrapolation from the data. The black line represents a fit to the Venus data with the dashed part not considered in the fit.

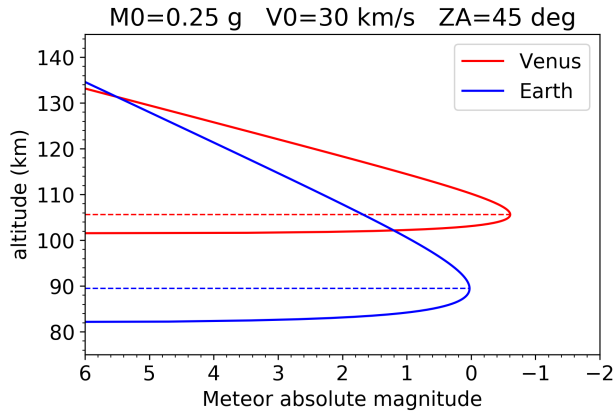


Figure 2: Magnitude-height profile for a meteoroid abating in the atmospheres of Venus and the Earth. The dashed lines indicate the heights of maximum light calculated from theory.

During ablation, the meteoroid cross-section S is assumed to depend on the remaining mass M as $S/S_0=(M/M_0)^\mu$ where $0<\mu<2/3$, the upper limit corresponding to a shape of the body being constant (self-similar) during the flight (Levin, 1956; Bouquet et al., 2014; Sansom et al., 2019; Moreno-Ibáñez et al., 2020).

The right-hand-side in Eq. 4 vanishes at $\bar{\rho}=0$ and at $\bar{\rho}(h_{end})=K^{-1}$, h_{end} being the meteor ending height. By differentiating (4) wrt h and expressing the result as a function of $\bar{\rho}$, we obtain the height of *maximum light*:

$$\bar{\rho}(h_{max}) = (1 - \mu)K^{-1}. \quad (6)$$

Eqs 1 & 3 show that, all else being equal, meteor brightness is determined by the atmospheric density ρ_a . While the Earth's atmosphere is quasi-exponential from the surface up to $h>100$ km (Fig. 1), at Venus the characteristic scale height decreases from the lower to the middle atmosphere, then remains fairly constant up to ~ 130 km. Consequently,

despite the ~ 2 -orders-of-magnitude Venus/Earth surface density difference, respective density values are similar above ~ 100 km (Minzner, 1976; Seiff, 1983).

In the Earth's atmosphere, meteors typically appear at 80–110 km (Jenniskens, 2006) while at Venus, the same values of atmospheric density are encountered at 105–125 km. To apply the meteor model, we fitted the Venus data from Seiff (1983) to the function $\rho_a = \rho_0 \exp(-h/h_0)$. The resulting fit (black line) has $h_{0V} = 4.0$ km and $\rho_{0V} = 2.53 \times 10^6$ kg m $^{-3}$. For the Earth, we adopt the values (Bouquet et al., 2014, see also Gritsevich and Stulov (2006) and Moreno-Ibáñez et al. (2015)): $h_{0E} = 7.16$ km and $\rho_{0E} = 1.29$ kg m $^{-3}$.

The expression for the dimensionless coefficient K (Eq. 5) depends on parameters such as c_h and H^* that are poorly constrained from observations and often hinder the computation process. However, K can also be expressed as $K=2\alpha\beta$, where the ballistic coefficient α and mass loss parameter β admit to straightforward physical interpretations (Stulov, 1997; Moreno-Ibáñez et al., 2020). These parameters can be directly derived for each meteor from the observations, eliminating the need for prior knowledge of the poorly constrained parameters (Gritsevich, 2009; Lyytinen and Gritsevich, 2016; Sansom et al., 2019; Boaca et al., 2022). Given the absence of meteor observations in the Venusian atmosphere for inversion studies and our aim to forward-model the meteor lightcurves, we re-parameterise K in terms of the ablation coefficient $\sigma=c_h/c_d H^*$ and the shape factor $A_0=S_0\rho_m^{2/3}/M_0^{2/3}$ of a meteoroid when it enters the atmosphere, to obtain

$$K = \frac{(1 - \mu) c_d A_0 \sigma \rho_0 h_0 V_0^2}{2 M_0^{1/3} \rho_m^{2/3} \sin \gamma}. \quad (7)$$

The product $c_d A_0$ of the initial shape factor and the drag coefficient in Eq. 7 is often assumed to fall within the range 1.55–1.8 for a realistically shaped body (Gritsevich and Popelenskaya, 2008; Gritsevich et al., 2017; Shober et al., 2022) and equals 1.21 for an initially spherical meteoroid.

Eqs. 1, 4 & 7 can now be used to generate meteor lightcurves for small meteoroids of various speeds and masses. Figure 2 shows such a lightcurve for an initial mass $M_0=0.25$ g, density $\rho_m=1000$ kg m $^{-3}$, speed $V_0=30$ km s $^{-1}$ and $\gamma=45^\circ$. The meteoroid luminous efficiency τ , ablation coefficient σ and μ were fixed at the values $\tau=1\%$, $\sigma=0.1$ s 2 km $^{-2}$ and $\mu=0.65$ respectively. Luminous intensity is converted to stellar magnitude through the expression (Ceplecha and Revelle, 2005; Gritsevich and Koschny, 2011)

$$m = -2.5 (\log_{10} I - 3.185) \quad (8)$$

with I expressed in W. The resulting meteor reaches $m \simeq +0^m$ at $h_{max,E} \simeq 89$ km in the Earth's atmosphere; the slightly brighter meteor at Venus has $h_{max,V} \simeq 106$ km.

Meteor observations at Venus

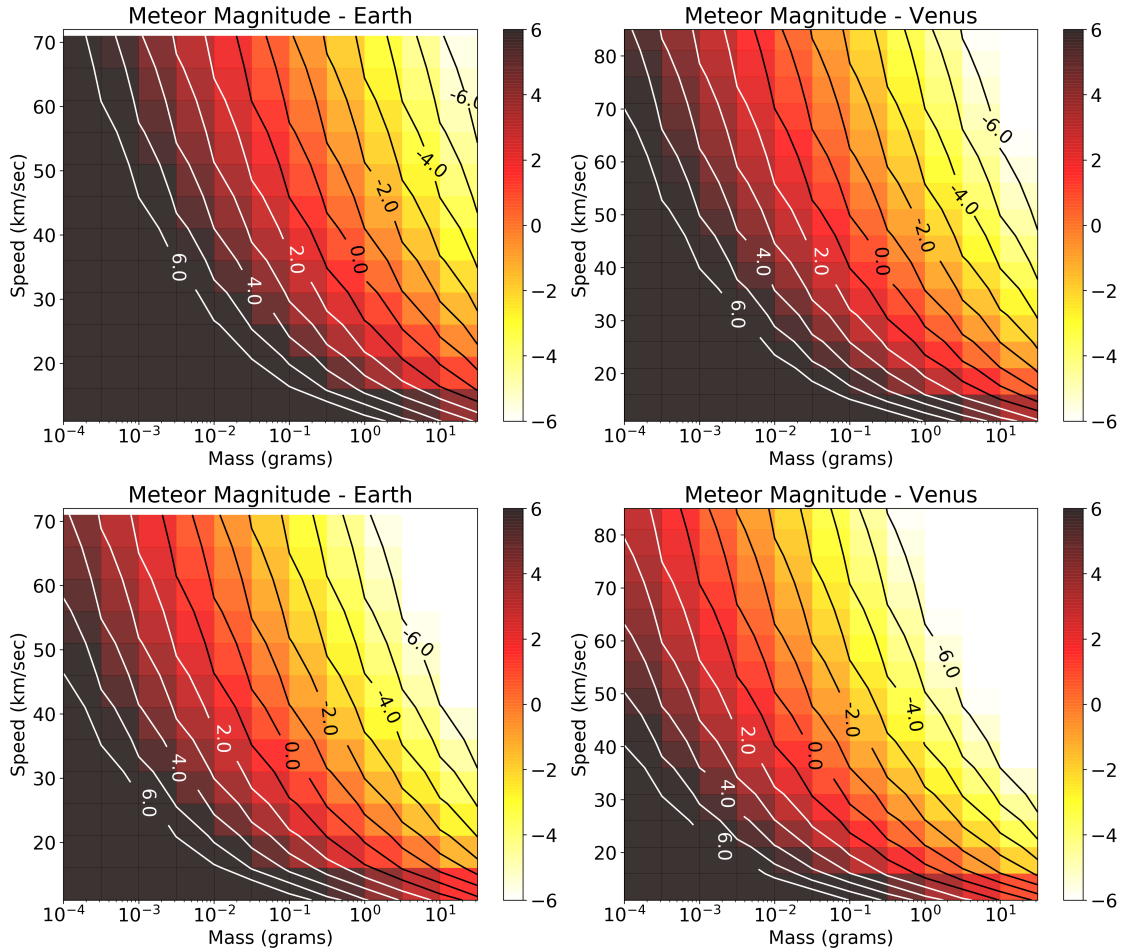


Figure 3: Maximum brightness of Earth and Venus meteors for a meteoroid density of 500 kg m^{-3} (top) and 2800 kg m^{-3} (bottom). Speed limits correspond to the planetary escape velocity (lower limit) and a head-on encounter with the planet while in a retrograde heliocentric orbit with perihelion at the planet's distance from the Sun (upper limit). See also Table 2.

It can be shown that, for a given set of meteoroid initial properties the relative maximum intensity of meteors at the two planets depends only on the ratio of atmospheric scale heights

$$\frac{I_{max,V}}{I_{max,E}} = \frac{h_{0E}}{h_{0V}} \quad (9)$$

or $\Delta m = -0^m.63$ (Eq. 8) therefore meteoroids of the same mass, density and speed at Venus will always produce brighter but shorter-lived meteors than their terrestrial counterparts. Model brightnesses as functions of mass and speed are shown in Fig. 3 for meteoroid bulk densities of 500 and 2800 kg m^{-3} , used here to represent cometary and asteroidal material respectively. These values are in good agreement with the ablation simulations of McAuliffe and Christou (2006) that used the actual atmospheric density-height profiles from Seiff (1983). Those authors reported

Meteor observations at Venus

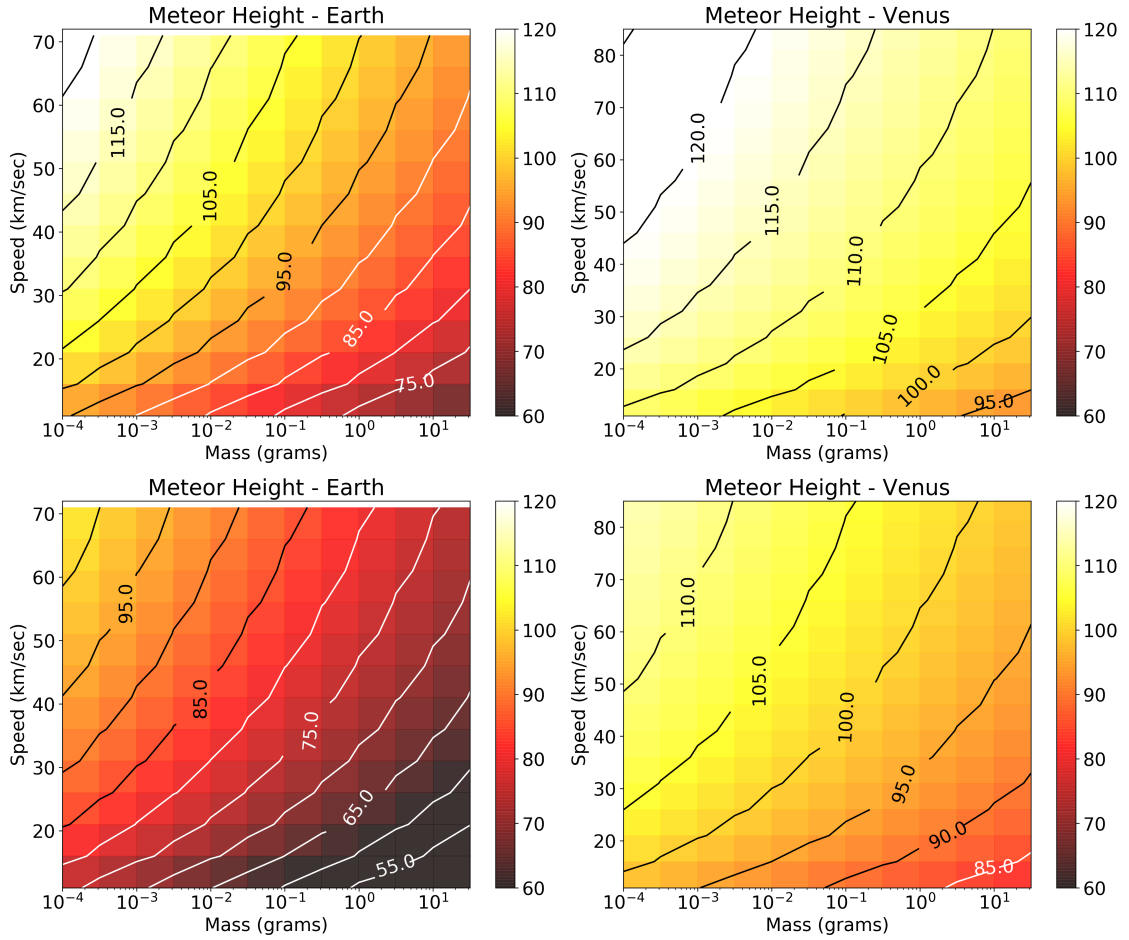


Figure 4: Height at maximum brightness for Earth and Venus meteors for meteoroid densities of 500 kg m^{-3} (top) and 2800 kg m^{-3} (bottom). A brighter colour indicates a higher altitude.

Earth – Venus differences between $+0.4^{\text{m}}$ and $+0.7^{\text{m}}$ for high-density rocky material while the same differences for low-density icy material and masses $< 10^{-4} \text{ g}$ were higher, $> +1.0^{\text{m}}$.

Similarly, we find that model peak ablation *heights* of terrestrial meteors are 75–120 km in the cometary case and 55–100 km in the asteroidal case (Fig. 4). Theory predicts higher ablation heights at Venus and, for the same mass and speed ranges, we find these to be 95–125 km for cometary meteors and 85–110 km for asteroidal meteors. These brightness and height values are again in very good agreement with the ablation simulations of McAuliffe and Christou (2006) for meteoroids in the same entry mass and speed ranges.

Actually, in the exponential atmosphere approximation there is a locus of points in (M_0, V_0) space where $\Delta h_{\text{max}}=0$, i.e. the ablating meteoroids reach maximum luminosity at the same common altitude h_C in the two atmospheres. This

follows from setting $h_{max}=h_{V,max}=h_{E,max}$ in Eq. 6, obtaining the expression

$$h_C = \frac{h_{0E}h_{0V}}{h_{0E} - h_{0V}} \log \left(\frac{\rho_{0E}h_{0E}}{\rho_{0V}h_{0V}} \right) \quad (10)$$

that evaluates to $h_C=125.9$ km using the atmospheric parameter values in this paper. Moreover, we have that $|h_V - h_C| < |h_E - h_C|$, in other words Venus meteors reach maximum brightness within a narrower range of altitudes than at Earth. As the Venusian atmosphere is cloud- and haze-free above 90 km altitude (Titov et al., 2018), meteor surveys from orbiters around Venus appear feasible, a conclusion also reached by McAuliffe and Christou (2006).

3. Simulating meteor surveys from orbit

To assess the performance of a meteor camera onboard a Venus orbiter, we utilize SWARMS (Simulator for Wide Area Recording of Meteors from Space), a python-based numerical tool designed to simulate the detection of meteors with space-based optical sensors (Bouquet, 2013; Bouquet et al., 2014). The tool incorporates analytical equations developed through a physics-based parameterisation to characterize the variations in mass, height, velocity, and luminosity of a meteor along its atmospheric trajectory (Gritsevich, 2007, 2009; Gritsevich and Koschny, 2011; Peña-Asensio et al., 2021). Observations are assumed to take place from a circular orbit at a fixed altitude H above the planetary surface, while the detector itself is parameterised by the field of view (FOV), meteor limiting magnitude (m_{lim}), exposure time (T) and the minimum number of frames (ND) required for a valid detection. The meteoroid influx is modelled by sampling user-defined statistical distributions of number influx vs mass, of the bulk density and of the entry speed. The surface of the planet is represented by a mesh of equal-area flat elements with the meteor generation and detection algorithms applied only to those mesh elements within the detector field of view and on the planetary hemisphere below the observer.

SWARMS regards meteors as detected if they exceed a luminosity threshold I_{min} for at least $ND \times T$ sec. To simplify the detection decision, lightcurves are assumed gaussian in shape and an empirical factor F is introduced so that detection is determined from the total luminous energy E , if

$$E > I_{min} \times T \times ND \times F \quad (11)$$

with $E = \tau_G E_{kin}$, E_{kin} being the initial kinetic energy.

In the simulations reported in Bouquet et al. (2014), both τ_G and F are determined by applying the ablation theory of Gritsevich (2009) and Gritsevich and Koschny (2011) to the fireball data of Halliday et al. (1996). Specifically, τ_G

is defined through the empirical function

$$\tau_G = 0.0051(V_0 - 10 \text{ km s}^{-1})^{0.87}(100\sigma)^{-1.46} \quad (12)$$

where V_0 is the atmospheric entry speed and the ablation coefficient σ is estimated from the meteoroid density ρ_m (Revelle and Ceplecha, 2001; Bouquet et al., 2014) as

$$\sigma = \log_{10}(\rho_m - 0.25)/4.77/23.5 \quad (13)$$

while the value $F=F_E=18.51$ is adopted for the empirical scale factor in Eq 11. Meteoroid speeds in SWARMS follow the log-normal distribution determined from meteor radar observations (Hunt et al., 2004):

$$\log_{10} V_0 \sim N(\log_{10} \mu_V, \log_{10}^2 \sigma_V) \quad (14)$$

where $N(\cdot)$ is the standard notation for the two-parameter gaussian probability density function with parameter values $\mu_V=20 \text{ km s}^{-1}$ and $\sigma_V=1.35 \text{ km s}^{-1}$. Typical speeds for the respective sporadic populations at the two planets should not differ by more than a few km s^{-1} (Carrillo-Sánchez et al., 2020), therefore we adopt the same distribution for the Venus runs. Likewise, we adopt the Bouquet et al. distribution for the meteoroid bulk density, so that its values are randomly and uniformly chosen between 1000 and 4000 kg m^{-3} . While meteoroids with density outside this range are abundant in the observational record e.g. cometary particles with density $<1000 \text{ kg m}^{-3}$ (Ceplecha et al., 1998), the adopted distribution represents an acceptable compromise between simulation realism and efficient representation of the principal meteoroid types in the calculation of τ_G and σ (Eq. 12 and 13 resp., see also Table 5 in Revelle and Ceplecha, 2001).

The SWARMS reference distribution for the meteoroid number influx is that of Halliday et al. (1996), obtained from a dataset of fireballs showing noticeable deceleration with absolute magnitudes m between -4 and -13 . These magnitudes are somewhat brighter than those of detectable meteors in our simulations ($m < +5$). Moreover, the mass index value of 1.48 obtained from the fireball data is rather low compared to values closer to ~ 2 reported for these fainter meteors (Ceplecha et al., 1998; Jenniskens et al., 2016). For these reasons, we adopt here a different meteoroid influx reference distribution for our SWARMS simulations than in Bouquet et al. (2014). The new distribution uses the collated data in Ceplecha et al. (1998) presented as a cumulative distribution of the annual meteoroid number influx to the Earth with masses in the range 10^{-18} – 10^{18} g (cf Table 26). To produce a law suited to our purposes we fitted the

Meteor observations at Venus

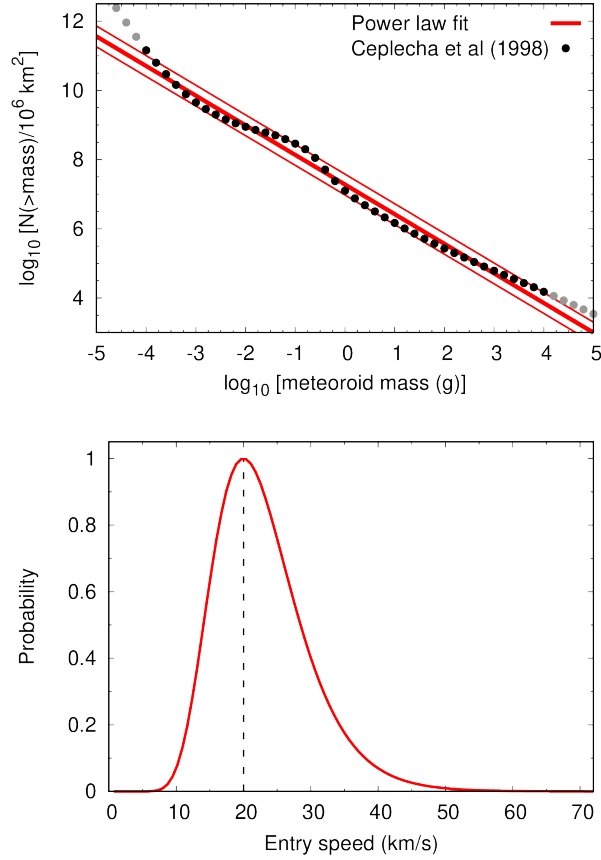


Figure 5: Statistical distributions used in SWARMS. Top: Power-law fit (Eq. 16) to the flux data in Ceplecha et al. (1998). The parallel lines indicate factor-of-two differences from the fit prediction. Grey data points were not considered in the fit. Bottom: Probability density function of the entry speed with a mode $\langle v \rangle = \mu_V = 20 \text{ km s}^{-1}$.

function

$$\log_{10} N(> M_0) = a + b \log_{10} M_0 \quad (15)$$

to these data within the mass interval 10^{-4} – 10^4 g, yielding $a=7.230 \pm 0.033 \log N(> 1\text{g})/\text{Earth}/\text{yr}$ and $b=-0.856 \pm 0.014$.

Masses outside this range were not considered in the fit as they do not contribute to meteor detections in the simulations.

By further assuming a fixed meteor altitude $h=90$ km at Earth we obtain the following expression for the number influx per yr and per 10^6 km^2 of atmospheric surface area:

$$\log_{10} N(> M_0) = 4.559 - 0.856 \log_{10} M_0 \quad (16)$$

This relationship reproduces the Ceplecha et al. data to within a factor of two (Fig. 5), with the worst agreement observed for $M_0 \approx 10^{-4}$ g (equivalent meteoroid diameter of 0.6 mm for a 1000 kg m^{-3} bulk density).

Table 2
Planetary characteristics used in the simulations.

Property	Earth	Venus
Mass ($\times 10^{24}$ kg)	5.97	4.87
Radius (km)	6378	6051
Meteor altitude (km)	90	110
Escape speed (km s^{-1})	11.10	10.27
Maximum pre-atmospheric speed (km s^{-1})	72.8	85.2

Table 3
Characteristics of camera systems in this study.

Property	SPOSH	Mini-EUSO
Field of view ($^{\circ}$)	120	40
Limiting magnitude	+6	+5
Exposure time (s)	0.06	0.04
Angular speed ($^{\circ} \text{s}^{-1}$)	5	5

We then apply SWARMS to either Earth or Venus orbiters by adopting the appropriate set of parameter values from Table 2 combined with the stated influx, speed and density distributions for the meteoroids.

Furthermore, we utilise the constant-scale-height fits to the atmospheric profiles shown in Fig. 1 and divide the scale factor F_E in Eq 11 by the ratio h_{0E}/h_{0V} to obtain the value $F_V=10.34$ to be used for determining whether a meteor is detectable or not from an orbiter at Venus. No atmospheric extinction correction is applied to the apparent brightness of simulated meteors. We expect this to be negligible for typical meteor heights at Earth and Venus (Fig 4) when observation takes place from above the atmosphere as is the case here. The simulated survey duration in each of our SWARMS runs is varied from a few hours to several weeks, as appropriate to accumulate a sufficiently high number of detections - at least several hundreds - to ensure a statistically robust outcome. This number is then divided by the survey duration to obtain the hourly detection rate for that run. Finally, we do not consider the effects of spatial or temporal variations in the terrestrial and venusian sporadic rate. Although such variations likely exist at both planets (Campbell-Brown, 2007; Janches et al., 2020), it is not clear to us that they are significant enough to alter the outcome of this study.

4. Scientific use cases: SPOSH and Mini-EUSO

Apart from the model meteoroid population and the observation circumstances, the degree of realism in our simulations depends on selecting detector characteristics appropriate for the task. A wide field of view, high sensitivity, and a rapid frame rate are all essential requirements for the efficient optical detection of meteors, yet instrumentation with flight heritage seldom features these in combination.

Meteor observations at Venus

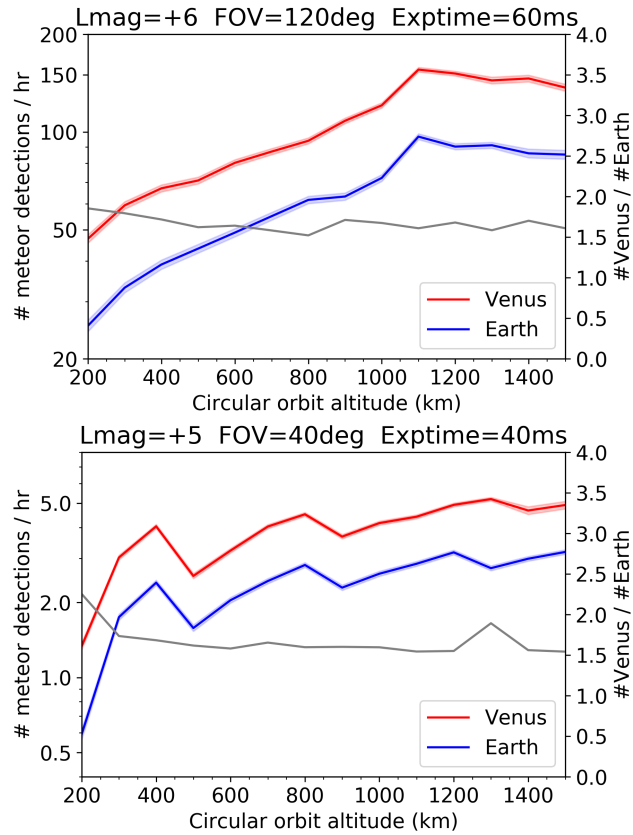


Figure 6: Hourly rate of meteor detections at Earth and Venus for detectors with similar characteristics to SPOSH (top) and Mini-EUSO (bottom). The gray line represents the ratio of the number of meteors detected at the two planets.

Recent interest in detecting fast optical transients in the Earth’s atmosphere from space has yielded two facility concepts suitable for the task: the Smart Panoramic Optical Sensor Head (SPOSH; Oberst et al., 2011; Christou et al., 2012) and the Joint Exploratory Missions for an Extreme Universe Space Observatory (JEM-EUSO; Haungs and the JEM-EUSO collaboration, 2015). Breadboard versions of SPOSH were successfully field-tested in a two-station configuration, completing a multi-year survey of the Perseid meteor shower (Margonis et al., 2019) while the JEM-EUSO study evolved into the Mini-EUSO demonstrator that has been systematically recording meteors from the International Space Station since 2019 (Bacholle et al., 2021; Coleman et al., 2023).

The principal characteristics of SPOSH and Mini-EUSO are listed in Table 3. The SPOSH camera, also adopted by Bouquet et al. in their study, was specifically designed to detect meteors from orbital altitudes (Oberst et al., 2011) while Mini-EUSO was developed as a proof-of-concept optical transient detector on the International Space Station under the JEM-EUSO project (Coleman et al., 2023). Operating in the ultraviolet part of the electromagnetic spectrum (290–430 nm) and designed to detect meteors of apparent magnitude +5 or brighter under dark background conditions (Abdellaoui et al., 2017), Mini-EUSO has been operating since 2019 mounted on the ISS *Zvezda* module at an altitude of 400 km above the Earth’s surface (Bacholle et al., 2021). The actual flight model features a slightly larger FOV than

Meteor observations at Venus

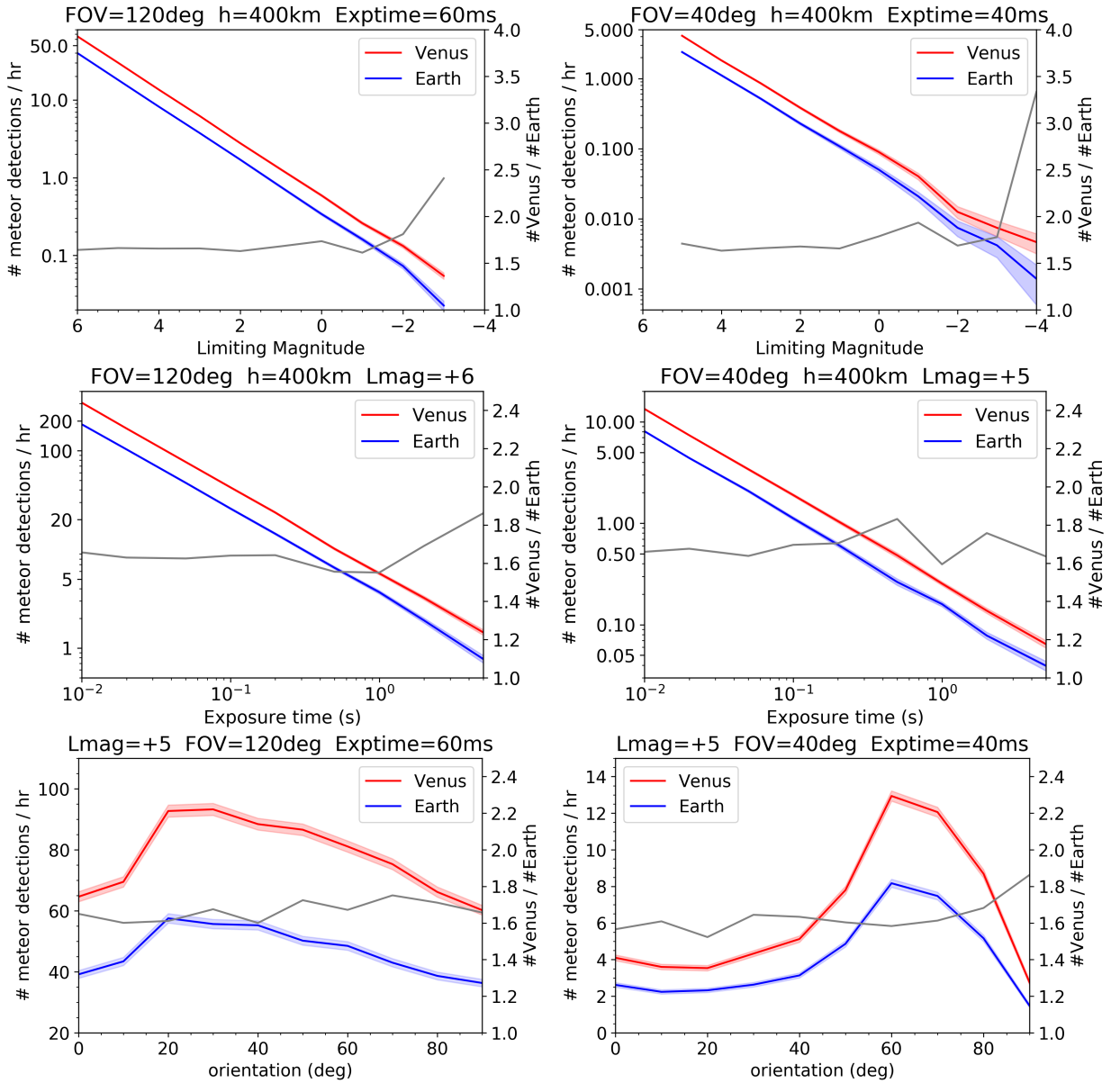


Figure 7: Hourly rate of meteor detections at Earth and Venus as a function of camera limiting magnitude (top), exposure time (middle) and orientation (bottom) for SPOSH (left column) and for Mini-EUSO (right column).

the original design, however for our simulations we adopted the design value of 40° . Figure 6 shows the simulation output for both use cases and for a range of orbital altitudes at Earth and Venus. Narrow shaded bands that accompany each line represent $1\text{-}\sigma$ Poisson counting uncertainties from the simulation output. Consistent with the analysis in Section 2, more meteors are generally detected at Venus than at Earth. The detection rate ratio (grey line) takes values in the range 1.5–2.0 for each camera and is fairly independent of altitude. The primary difference between the use cases is a higher detection rate for SPOSH (25–150 hr^{-1}) compared to Mini-EUSO (0.6–5 hr^{-1}) owing to the much wider field of view of the former. The character of the altitude dependence is also different; for SPOSH the detection rate

gradually increases until $h \sim 1100$ km and remains approximately constant thereafter, while the Mini-EUSO detection rate is roughly constant for $h \gtrsim 300$ km following a rapid increase.

The initial increase is likely due to the larger atmospheric surface area surveyed, where this effect dominates over the loss of fainter meteors due to the increasing distance. With a further increase in altitude for the wider-field SPOSH, the planet eventually fills the field of view, leading to the change in slope observed at 1100 km.

5. Sensitivity analysis

5.1. Detector characteristics

A separate batch of simulations was run to study how the detection rate varies with camera characteristics. We focused on three parameters in particular: limiting magnitude, frame exposure time and angle between the boresight and the nadir direction. This quantity is the tilt angle in Bouquet et al. (2014) but here we refer to it as the *orientation* angle. For the simulations in this and the next subsection the observation orbit altitude was fixed at $H=400$ km.

We again find (Fig. 7) that the detection rate ratio is unaffected by the changes, varying between 1.5 and 2.5. The absolute detection rate at either planet is a log-linear function of the sensitivity and of the exposure time (top and middle panels respectively), decreasing by an order of magnitude for every ~ 3 -magnitude reduction in camera sensitivity or an order-of-magnitude increase in exposure time length. The variation with orientation angle (bottom panels) is more modest by contrast. Our SPOSH simulations show variation within a factor of $1.5\times$ peaking at an orientation angle of $\sim 30^\circ$ while the Mini-EUSO runs show a more pronounced, $3\times$ variation peaking at $\sim 60^\circ$, similar to that noted in Bouquet et al. (2014) for a 60° FOV. These extrema correspond to the maximum atmospheric surface area under observation, again highlighting the relative importance of area coverage over range in attempting to detect meteors from orbit.

5.2. Meteoroid population parameters

The model meteoroid population in the simulations is parameterised by the mass index s of the power law that describes the meteoroid flux and by the parameters of the atmospheric entry speed distribution, particularly the mode $\langle v \rangle$. Both these parameters are unconstrained by direct observations at Venus and it is of interest to determine how varying either s or $\langle v \rangle$ affects the outcome.

Figure 8 shows the change in the detection rate with altitude for different values of s with the result for the reference value (dashed line) included for comparison. We find that the relative number of detections at lower vs higher altitudes increases with increasing s with the curves flattening out at $s=2$. This flat distribution ($< 2\times$ variation at all altitudes) shows that, in this case, the gain in area coverage almost exactly compensates for the loss of the fainter meteors. This feature also appears in our results for Earth (not shown here) and may be a general characteristic of the observation of

Meteor observations at Venus

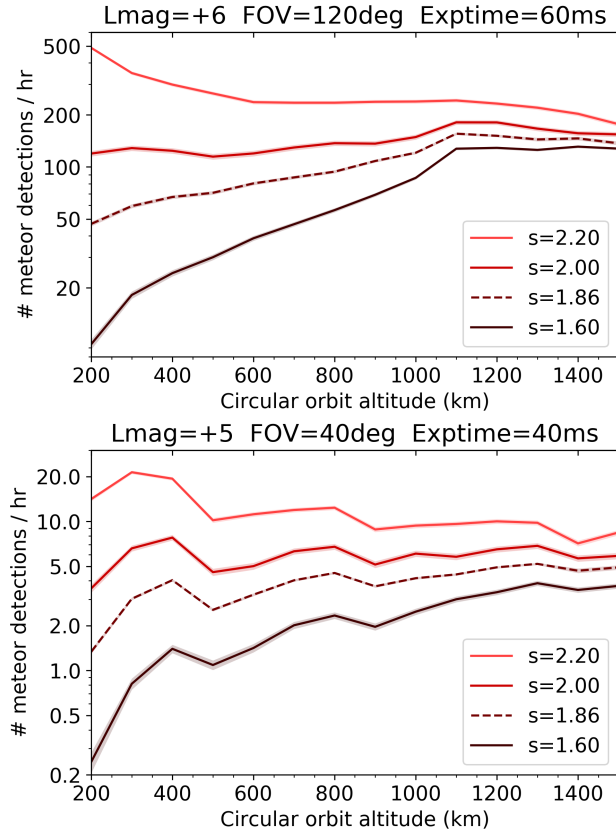


Figure 8: Hourly rate of meteor detections at Venus for SPOSH (top) and Mini-EUSO (bottom) for different values of the meteoroid mass index s where a brighter colour indicates a steeper mass distribution.

meteors from space-based platforms. It also means that observational characterisation of meteoroid populations with low s such as meteor showers would benefit from the wider area coverage available at higher altitudes (but see below), or by pointing the camera near the planetary limb (Fig. 7) as in the 1997 Leonid observations (Jenniskens et al., 2000). Increasing the meteoroid speed yields a significant increase in meteor brightness because of the steep dependence of the ablation rate on this parameter (Eq. 3). We therefore expect the detection rate to also increase. Simulation runs with different values of the mode $\langle v \rangle$ of the particle speed distribution (Fig. 9) indeed show an increase by $1.8\times$ at all altitudes for every incremental change in this parameter by 5 km s^{-1} . This finding has implications for the efficient detection of Halley-Type and Long-period Comet meteor showers at Venus, with entry speeds between 50 and 80 km s^{-1} (Beech, 1998; Christou, 2010). Specifically, the corresponding 2- to 3-orders-of-magnitude increase in detection rate for these fast meteors should compensate for their relatively inefficient detection from low altitude orbits due to generally shallow mass distributions.

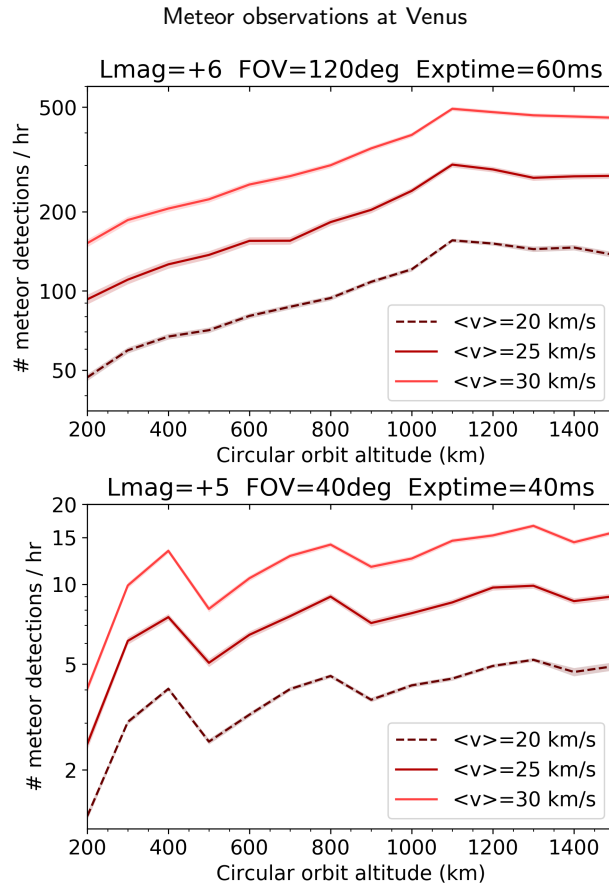


Figure 9: Hourly rate of meteor detections at Venus for SPOSH (top) and Mini-EUSO (bottom) for different values of the mode $\langle v \rangle$ of the speed distribution (Eq. 14) where a brighter colour indicates a faster population of meteoroids.

6. Conclusions and Discussion

This work investigated the feasibility of detecting meteors in the atmosphere of Venus from an orbiter. By applying a physical model of the production of meteor light during the atmospheric ablation of a meteoroid we showed that Venus meteors would be moderately brighter, shorter-lived and appear higher in the atmosphere than Earth meteors, the principal cause for these differences being the different density scale heights of the atmospheres. We then carried out orbital survey simulations using the SWARMS s/w, showing that such surveys would yield a higher (by $1.5\times$ – $2.5\times$) rate of detections at Venus over Earth. That fact, and the relative accessibility of Venus compared to other solar system planets or satellites with an atmosphere make this planet an ideal venue to conduct the first non-terrestrial meteor survey. Such a survey holds many benefits, including the significant expansion of the observational sample volume in the solar system for potential detection of interstellar meteors, a topic currently under debate in scientific discussions (Pēna-Asensio et al., 2024).

The quantitative estimates drawn from our study are, strictly speaking, valid under the specific assumptions defining detector performance, observation orbit, the characteristics of incoming meteoroids and the atmospheric density model.

Therefore further simulations were conducted to quantify the parametric dependence of the outcomes. Our findings indicate that the Venus-Earth detection ratio remains consistent and is largely insensitive to variations in the chosen observation orbit and detector characteristics.

EnVision, an orbital mission to Venus developed by the European Space Agency (Wilson et al., 2022; Widemann et al., 2023), will perform high-resolution radar mapping and atmospheric observations from a near-circular 220×570 km science orbit¹ that closely resembles the baseline 400-km circular orbit in our simulations. Our simulation results can therefore be directly used to quantify the performance of a hypothetical meteor camera onboard that spacecraft.

For a rough estimate of the detection rate at Venus, let us assume an instrument with the same performance characteristics and duty cycle as Mini-EUSO and further require that a survey should, at a minimum, aim to yield a sufficient number of detections to measure the population indices - in other words, the relative abundance of faint over bright meteors - of the sporadic background and of the principal showers at Venus. Marcelli and the JEM-EUSO Collaboration (2023) report a Mini-EUSO detection tally of 24,000 meteors over 90 12-hr sessions on the ISS or ~22 meteors hr⁻¹ which we convert to a Venus detection rate of 33–55 meteors hr⁻¹ using our findings. If we further assume that (i) shower meteors comprise ~1/3 of the total influx of detectable meteors (Jenniskens et al., 2016), (ii) a sample of 50 or more meteors per shower - somewhat more than the 29 Leonids detected from space in 1997 (Jenniskens et al., 2000) - is sufficient to estimate the shower population index, and (iii) there exist ~10 strong showers at Venus, we estimate that a survey would require to detect ~10×50+1000 = 1500 meteors over a period of one Venus year (~225d), an average rate of 0.28 meteors hr⁻¹. This exceeds our projected detection rate at Venus by ≳2 orders of magnitude and shows that even a less capable version of the instrument - for instance, one featuring a brighter limiting magnitude, a longer single-frame exposure time or a lower duty cycle - will comfortably achieve the survey objectives.

An added complication at Venus is that the data return strategy adopted for Mini-EUSO at the ISS, where the full dataset is stored in memory cards that then are physically returned to Earth for analysis, is not feasible at Venus requiring the availability of appropriate on-board processing to identify and store the relatively small fraction of camera footage containing meteor events for later transmission to Earth. In this context, we note that efficient algorithms for real-time capture and storage of meteor footage have been in use by the meteor community for many years (Yamamoto, 2005; Atreya and Christou, 2008; Blaauw and Cruse, 2012; Guennoun et al., 2019). These may serve as suitable starting points to develop the needed capability.

Declaration of competing interests

The authors have no known competing financial interests or personal relationships that could have appeared to influence the work reported in this paper.

¹https://www.esa.int/Science_Exploration/Space_Science/EnVision_factsheet

Data availability

Data will be made available upon reasonable request.

Acknowledgements

We thank the two anonymous reviewers whose critical reading of the manuscript improved the presentation of this work. Astronomical research at the Armagh Observatory & Planetarium is grant-aided by the Northern Ireland Department for Communities (DfC). We are grateful to the Academy of Finland and the Finnish Geospatial Research Institute for supporting the project no. 325806 (PlanetS), which facilitated the development of the modelling approaches utilized in this paper. The program of development within Priority-2030 is acknowledged for supporting the research at UrFU. We thank Dr. Alexis Bouquet for valuable discussions during the development of his Master Thesis and for sharing the earlier version of the SWARMS code, which proved instrumental in implementing our programme of simulations.

References

- Abdellaoui, G., Abe, S., 358 co-authors, 2017. Meteor studies in the framework of the JEM-EUSO program. *Planet. Space Sci.* 143, 245–255. doi:10.1016/j.pss.2016.12.001.
- Asher, D.J., Bailey, M.E., Emelyanenko, V.V., 1999. Resonant meteoroids from Comet Tempel-Tuttle in 1333: the cause of the unexpected Leonid outburst in 1998. *Mon. Not. R. Astron. Soc.* 304, L53–L56. doi:10.1046/j.1365-8711.1999.02615.x.
- Atreya, P., Christou, A.A., 2008. The Armagh Observatory meteor camera cluster: Overview and status. *Earth, Moon & Planets* 102, 263–267. doi:10.1007/s11038-007-9170-6.
- Bacholle, S., Barrillon, P., 59 co-authors, 2021. Mini-EUSO mission to study Earth UV emissions on board the ISS. *Astrophys. J. Suppl. Ser.* 253, 36. doi:10.3847/1538-4365/abd93d.
- Beech, M., 1998. Venus-intercepting meteoroid streams. *Mon. Not. R. Astron. Soc.* 294, 259–264. doi:10.1046/j.1365-8711.1998.01178.x.
- Beech, M., 2006. *Meteors and meteorites: Origins and observations*. Crowood Press, United Kingdom.
- Beech, M., Brown, P.J., 1995. On the visibility of bright Venusian fireballs from Earth. *Earth, Moon & Planets* 68, 171–179. doi:10.1007/BF00671506.
- Blaauw, R., Cruse, K.S., 2012. Comparison of ASGARD and UFOCapture, in: *Proceedings of the International Meteor Conference, Sibiu, Romania, 15-18 September, 2011, International Meteor Organisation*. pp. 44–46.
- Blaske, C., Borrelli, M., O'Rourke, J., Desch, S., 2023. Meteors may masquerade as lightning in the atmosphere of Venus. *JGR Planets* 128, e2023JE007914. doi:10.1029/2023JE007914.
- Boaca, I., Gritsevich, M., Birlan, M., Nedelcu, A., Boaca, T., Colas, F., Malgoyre, A., Zanda, B., Vernazza, P., 2022. Characterization of the fireballs detected by all-sky cameras in romania. *Astrophys. J.* 936, 150. doi:10.3847/1538-4357/ac8542.
- Bouquet, A., 2013. *Simulator for monitoring of meteors from orbit*. MSc Thesis, Université Paul Sabatier Toulouse.
- Bouquet, A., Baratoux, D., Vaubaillon, J., Gritsevich, M.I., Mimoun, D., Mousis, O., Bouley, S., 2014. Simulation of the capabilities of an orbiter for monitoring the entry of interplanetary matter into the terrestrial atmosphere. *Planet. Space Sci.* 103, 238–249. doi:10.1016/j.pss.2014.

09.001.

- Bronshen, V.A., 1983. Physics of meteoric phenomena. Reidel, Dordrecht.
- Brown, P., Weryk, R.J., Wong, D.K., Jones, J., 2008. A meteoroid stream survey using the Canadian Meteor Orbit Radar. I. Methodology and radiant catalogue. *Icarus* 195, 317–339. doi:10.1016/j.icarus.2007.12.002.
- Campbell-Brown, M.G., 2007. The meteoroid environment: Shower and sporadic meteors, in: Krueger, H., Graps, A. (Eds.), Workshop on Dust in Planetary Systems, ESA SP-643. pp. 11–21.
- Carbary, J., Morrison, D., Romick, G.J., Yee, J.H., 2003. Leonid meteor spectrum from 110 to 860 nm. *Icarus* 161, 223–234. doi:10.1016/S0019-1035(02)00064-7.
- Carrillo-Sánchez, J.D., Gómez-Martín, J.C., Bones, D.L., Nesvorný, D., Pokorný, P., Benna, M., Flynn, G.J., Plane, J.M.C., 2020. Cosmic dust fluxes in the atmospheres of Earth, Mars, and Venus. *Icarus* 335, 113395. doi:10.1016/j.icarus.2019.113395.
- Carrillo-Sánchez, J.D., Nesvorný, D., Pokorný, P., Janches, D., Plane, J.M.C., 2016. Sources of cosmic dust in the Earth's atmosphere. *Geophys. Res. Lett.* 43, 11,979–11,986. doi:10.1002/2016GL071697.
- Ceplecha, Z., Borovička, J., 5 co-authors, 1998. Meteor phenomena and bodies. *Space Sci. Rev.* 84, 327–471. doi:10.1023/A:1005069928850.
- Ceplecha, Z., Revelle, D.O., 2005. Fragmentation model of meteoroid motion, mass loss, and radiation in the atmosphere. *Met. Planet. Sci.* 40, 35–54. doi:10.1111/j.1945-5100.2005.tb00363.x.
- Christou, A.A., 2004a. Predicting martian and venusian meteor shower activity. *Earth Moon & Planets* 95, 425–431. doi:10.1007/s11038-005-9023-0.
- Christou, A.A., 2004b. Prospects for meteor shower activity in the venusian atmosphere. *Icarus* 168, 23–33. doi:10.1016/j.icarus.2003.12.006.
- Christou, A.A., 2010. Annual meteor showers at Venus and Mars: lessons from the Earth. *Mon. Not. R. Astron. Soc.* 402, 2759–2770. doi:10.1111/j.1365-2966.2009.16097.x.
- Christou, A.A., Oberst, J., 9 co-authors, 2007. Comparative studies of meteoroid-planet interaction in the inner solar system. *Planet. Space Sci.* 55, 2049–2062. doi:10.1016/j.pss.2007.05.001.
- Christou, A.A., Oberst, J., Elgner, S., Flohrer, J., Margonis, A., McAuliffe, J.P., Koschny, D., 2012. Orbital observations of meteors in the Martian atmosphere using the SPOSH camera. *Planet. Space Sci.* 60, 229–235. doi:10.1016/j.pss.2011.09.002.
- Christou, A.A., Vaubaillon, J., 2010. Modelling an encounter between a spacecraft and a cometary meteoroid trail in interplanetary space: The case of the Venus Climate Orbiter and comet 27P/Crommelin. *Planet. Space Sci.* 58, 1026–1034. doi:10.1016/j.pss.2010.03.008.
- Christou, A.A., Vaubaillon, J., Withers, P., Hueso, R., Killen, R., 2019. Extraterrestrial meteors, in: Ryabova, G.O., Asher, D.J., Campbell-Brown, M.G. (Eds.), *Meteoroids: Sources of Meteors on Earth and Beyond*. Cambridge University Press, Cambridge, pp. 119–135. doi:10.48550/arXiv.2010.14647.
- Coleman, A., Eser, J., 96 co-authors, 2023. Ultra high energy cosmic rays: The intersection of the cosmic and energy frontiers. *Astroparticle Physics* 147, 102794. doi:10.1016/j.astropartphys.2022.102794.
- Frankland, V., James, A.D., Carrillo-Sánchez, J.D., Nesvorný, D., Pokorný, P., Plane, J.M.C., 2017. CO oxidation and O₂ removal on meteoric material in Venus' atmosphere. *Icarus* 296, 150–162. doi:10.1016/j.icarus.2017.06.005.
- Gritsevich, M., Dmitriev, V., Vinnikov, V., Kuznetsova, D., Lupovka, V., Peltoniemi, J., Mönkölä, S., Brower, J., Popyrev, Y., 2017. Constraining the pre-atmospheric parameters of large meteoroids: Košice, a case study, in: *Astrophys. Space Sci. Proc.*, Springer International Publishing. p. 153. doi:10.1007/978-3-319-46179-3_8.

- Gritsevich, M., Nissinen, M., Oksanen, A., Suomela, J., Silber, E.A., 2022. Evolution of the dust trail of comet 17P/Holmes. *Mon. Not. R. Astron. Soc.* 513, 2201–2214. doi:10.1093/mnras/stac822.
- Gritsevich, M.I., 2007. Approximation of the observed motion of bolides by the analytical solution of the equations of meteor physics. *Solar System Research* 41, 509–514. doi:10.1134/S003809460706007X.
- Gritsevich, M.I., 2009. Determination of parameters of meteor bodies based on flight observational data. *Adv. Space Res.* 44, 323–334. doi:10.1016/j.asr.2009.03.030.
- Gritsevich, M.I., 2010. A new method for entry dynamics determination based on observations and results of calculations, in: *Proceedings of the International Meteor Conference, Barège, France, 7–10 June, 2007*, International Meteor Organisation. pp. 13–25.
- Gritsevich, M.I., Koschny, D., 2011. Constraining the luminous efficiency of meteors. *Icarus* 212, 877–884. doi:10.1016/j.icarus.2011.01.033.
- Gritsevich, M.I., Popelenskaya, N.V., 2008. Meteor and fireball trajectories for high values of the mass loss parameter. *Physics - Doklady* 53, 88–92. doi:10.1134/S1028335808020092.
- Gritsevich, M.I., Stulov, V.P., 2006. Extra-atmospheric masses of the Canadian Network bolides. *Solar System Research* 40, 477–484. doi:10.1134/S0038094606060050.
- Gritsevich, M.I., Stulov, V.P., Turchak, L.I., 2012. Consequences of collisions of natural cosmic bodies with the Earth's atmosphere and surface. *Cosmic Research* 50, 56–64. doi:10.1134/S0010952512010017.
- Grün, E., Zook, H.A., Fechtig, H., Giese, R.H., 1985. Collisional balance of the meteoritic complex. *Icarus* 62, 244–272. doi:10.1016/0019-1035(85)90121-6.
- Guenoun, M., Vaubaillon, J., Čapek, D., Koteš, P., Benkhaldoun, Z., 2019. A robust method to identify meteor showers new parent bodies from the SonotaCo and EDMOND meteoroid orbit databases. *Astron. Astrophys* 622, A84. doi:10.1051/0004-6361/201834593.
- Halliday, I., Griffin, A.A., Blackwell, A.T., 1996. Detailed data for 259 fireballs from the Canadian camera network and inferences concerning the influx of large meteoroids. *Met. Planet. Sci.* 31, 185–217. doi:10.1111/j.1945-5100.1996.tb02014.x.
- Hansell, S.A., Wells, W.K., Hunten, D.M., 1995. Optical detection of lightning on Venus. *Icarus* 117, 345–351. doi:10.1006/icar.1995.1160.
- Haungs, A., the JEM-EUSO collaboration, 2015. Physics goals and status of JEM-EUSO and its test experiments. *Journal of Physics: Conference Series* 632, 012092. doi:10.1088/1742-6596/632/1/012092.
- Huestis, D.L., Slanger, T.G., 1993. New perspectives on the Venus nightglow. *J. Geophys. Res.* 98, 10839–10847. doi:10.1029/93JE00997.
- Hunt, S.M., Oppenheim, M., Close, S., Brown, P.G., McKeen, F., Minardi, M., 2004. Determination of the meteoroid velocity distribution at the Earth using high-gain radar. *Icarus* 168, 34–42. doi:10.1016/j.icarus.2003.08.006.
- Janches, D., Bruzzone, J.S., Pokorný, P., Carrillo-Sánchez, J.D., Sarantos, M., 2020. A comparative modeling study of the seasonal, temporal, and spatial distribution of meteoroids in the upper atmospheres of Venus, Earth, and Mars. *Planet. Sci. J.* 1, id.59. doi:10.3847/PSJ/abba35.
- Jenniskens, P., 1994. Meteor stream activity I. The annual streams. *Astron. Astrophys.* 287, 990–1013.
- Jenniskens, P., 2006. *Meteor showers and their parent comets*. Cambridge University Press, Cambridge.
- Jenniskens, P., Nénon, Q., 8 co-authors, 2016. CAMS newly detected meteor showers and the sporadic background. *Icarus* 266, 384–409. doi:10.1016/j.icarus.2015.11.009.
- Jenniskens, P., Tedesco, E., Murthy, J., 2000. 1997 Leonid shower from space. *Earth, Moon & Planets* 82-83, 305–312. doi:10.1007/978-94-017-2071-7_23.
- Krüger, H., Kobayashi, M., Strub, P., Klostermeyer, G.M., Sommer, M., Kimura, H., Grün, E., Srama, R., 2021. Modelling cometary meteoroid stream traverses of the Martian Moons eXploration (MMX) spacecraft en route to Phobos. *Earth, Planets & Space* 73, id. 93. doi:10.1186/

s40623-021-01412-5.

- Levin, B.Y., 1956. *Physical Theory of Meteors and Meteoric Matter in the Solar System*. Acad. of Sci., U.S.S.R., Moscow.
- Lorenz, R., Takahashi, Y., Imai, M., Sato, M., 2022. Venus optical flash observed by the Akatsuki Lightning and Airglow Camera. *BAAS* 54, e-id. 2022n8i204p03.
- Lyytinen, E., Gritsevich, M., 2016. Implications of the atmospheric density profile in the processing of fireball observations. *Planet. Space Sci.* 120, 35–42. doi:10.1016/j.pss.2015.10.012.
- Marcelli, L., the JEM-EUSO Collaboration, 2023. Results and performance of the Mini-EUSO telescope on board the ISS. *Proceedings of Science*, eprint arXiv:2309.10630doi:10.48550/arXiv.2309.10630.
- Margonis, A., Christou, A., Oberst, J., 2019. Characterisation of the Perseid meteoroid stream through SPOSH observations between 2010-2016. *Astron. Astrophys.* 59, 1–9. doi:10.1051/0004-6361/201834867.
- McAuliffe, J., 2006. *Modelling meteor phenomena in the atmospheres of the terrestrial planets*. Ph.D. thesis. Queen’s University of Belfast.
- McAuliffe, J.P., Christou, A.A., 2006. Modelling meteor ablation in the venusian atmosphere. *Icarus* 180, 1–22. doi:10.1016/j.icarus.2005.07.012.
- McNaught, R.H., Asher, D.J., 1999. Leonid dust trails and meteor storms. *WGN, J. Int. Meteor Org.* 27, 85–102.
- Millman, P.M., 1963. A general survey of meteor spectra. *Smiths. Contr. Astrophys.* 7, 119–127.
- Minzner, R.A., 1976. Appendix B-The 1976 Standard Atmosphere and its relationship to earlier Standard Atmospheres, in: Minzner, R.A. (Ed.), *The 1976 Standard Atmosphere Above 86-km Altitude*, NASA SP-398. NASA, Washington, D.C., p. 51.
- Moreno-Ibáñez, M., Gritsevich, M., Trigo-Rodríguez, J.M., 2015. New methodology to determine the terminal height of a fireball. *Icarus* 250, 544–552. doi:10.1016/j.icarus.2014.12.027.
- Moreno-Ibáñez, M., Gritsevich, M., Trigo-Rodríguez, J.M., Silber, E.A., 2020. Physically based alternative to the PE criterion for meteoroids. *Mon. Not. R. Astron. Soc.* 494, 316–324. doi:10.1093/mnras/staa646, arXiv:2002.12842.
- Nesvorný, D., Janches, D.J., Vokrouhlický, D., Pokorný, P., Bottke, W.F., Jenniskens, P., 2011. Dynamical model for the zodiacal cloud and sporadic meteors. *Astrophys. J.* 743, 129. doi:10.1088/0004-637X/743/2/129.
- Nesvorný, D., Jenniskens, P., Levison, H.F., Bottke, W.F., Vokrouhlický, D., Gounelle, M., 2010. Cometary origin of the zodiacal cloud and carbonaceous micrometeorites: Implications for hot debris disks. *Astrophys. J.* 713, 816–836. doi:10.1088/0004-637X/713/2/816.
- Oberst, J., Flohrer, J., Elgner, S., Maue, T., Margonis, A., Schrödter, R., Tost, W., Buhl, M., Ehrich, J., Christou, A., Koschny, D., 2011. The Smart Panoramic Optical Sensor Head (SPOSH) - A camera for observations of transient luminous events on planetary night sides. *Planet. Space Sci.* 59, 1–9. doi:10.1016/j.pss.2010.09.016.
- Péna-Asensio, E., Visuri, J., Trigo-Rodríguez, J.M., Socas-Navarro, H., Gritsevich, M., Siljama, M., Rimola, A., 2024. Oort cloud perturbations as a source of hyperbolic Earth impactors. *Icarus* 408, 115844. doi:10.1016/j.icarus.2023.115844.
- Peña-Asensio, E., Trigo-Rodríguez, J.M., Gritsevich, M., Rimola, A., 2021. Accurate 3d fireball trajectory and orbit calculation using the 3d-firetoc automatic python code. *Mon. Not. R. Astron. Soc.* 504, 4829–4840. doi:10.1093/mnras/stab999.
- Revelle, D.O., Ceplecha, Z., 2001. Bolide physical theory and application to PN and EN fireballs, in: Warmbein, B. (Ed.), *Proceedings of the Meteoroids 2001 conference*, ESA SP-495. pp. 507–512.
- Sansom, E.K., Gritsevich, M., 8 co-authors, 2019. Determining fireball fates using the α - β criterion. *Astrophys. J.* 885, 115. doi:10.3847/1538-4357/ab4516, arXiv:1909.11494.
- Schimmerohn, M., Matura, P., Cardone, T., de Wilde, D., Krag, H., 2018. Numerical simulations for spacecraft catastrophic disruption analysis, in: *Clean Space Industrial Days 2018, ESTEC, 23-25 October 2018*, p. 18. URL: <https://indico.esa.int/event/234/contributions/>

3927/.

- Seager, S., Petkowski, J.J., 12 co-authors, 2022. Venus Life Finder habitability mission: Motivation, science objectives, and instrumentation. *Aerospace* 9, 733. doi:10.3390/aerospace9110733.
- Seiff, A., 1983. Appendix A. Models of Venus' atmospheric structure. In: Venus (Hunten, D.M., Colin, L., Donahue, T.M., Moroz, V.I., Eds.), 1045–1048.
- Shober, P.M., Devillepoix, H.A.R., 12 co-authors, 2022. Arpu Kuilpu: An H5 from the outer main belt. *Met. Planet. Sci.* 56, 1146–1157. doi:10.1111/maps.13813.
- Soja, R.H., Herzog, J.T., 10 co-authors, 2015. Meteor storms and showers with the IMEX model, in: Proceedings of the International Meteor Conference, Mistelbach, Austria, 27-30 August 2015, International Meteor Organisation. pp. 66–69.
- Stulov, V.P., 1997. Interactions of space bodies with atmospheres of planets. *Applied Mech. Rev.* 50, 671. doi:10.1115/1.3101678.
- Titov, D.V., Ignatiev, N.I., McGouldrick, K., Wilquet, V., Wilson, C.F., 2018. Clouds and hazes of Venus. *Space Sci. Rev.* 214, id. 126. doi:10.1007/s11214-018-0552-z.
- Valsecchi, G.B., Jopek, T.J., Froeschlé, C., 1999. Meteoroid stream identification: a new approach — I. Theory. *Mon. Not. R. Astron. Soc.* 304, 743–750. doi:10.1046/j.1365-8711.1999.02264.x.
- Vaubailion, J., Colas, F., Jorda, L., 2005a. A new method to predict meteor showers. I. Description of the model. *Astron. Astrophys.* 439, 751–760. doi:10.1051/0004-6361:20041544.
- Vaubailion, J., Colas, F., Jorda, L., 2005b. A new method to predict meteor showers. II. Application to the Leonids. *Astron. Astrophys.* 439, 761–770. doi:10.1051/0004-6361:20042626.
- Vaubailion, J., Ye, Q.Z., Egal, A., Sato, M., Moser, D.E., 2023. A new meteor shower from comet 46P/Wirtanen expected in December 2023. *Astron. Astrophys.* 680, L10. doi:10.1051/0004-6361/202348137.
- Widemann, T., Smrekar, S., 18 co-authors, 2023. Venus evolution through time: Key science questions, selected mission concepts and future investigations. *Space Sci. Rev.* 219, id. 56. doi:10.1007/s11214-023-00992-w.
- Wiegert, P., Vaubailion, J., Campbell-Brown, M., 2009. A dynamical model of the sporadic meteoroid complex. *Icarus* 201, 295–310. doi:10.1016/j.icarus.2008.12.030.
- Wilson, C.F., Widemann, T., Ghail, R., 2022. Venus: key to understanding the evolution of terrestrial planets. *Exp. Astron.* 54, 575–595. doi:10.1007/s10686-021-09766-0.
- Yamamoto, M., 2005. Recent meteor observing activities in Japan, in: Proceedings of the International Meteor Conference, Varna, Bulgaria, 23-26 September, 2004, International Meteor Organisation. pp. 104–109.